MATERIALE PLASTICE
https://revmaterialeplastice.ro
https://doi.org/10.37358/Mat.Plast.1964

Photothermal-Responsive PVA–GelMA@rGO Nanocomposite Hydrogel for Light-Controlled Anti-Inflammatory Drug Delivery in Neural Applications

ZHUHUAN SONG[1,#], DAWEI KONG[1,#], ZIHENG WANG[2], YONG HUANG[1], XIAOSONG WANG[1*]

[1] Department of Neurosurgery, Civil Aviation General Hospital, Beijing, China
[2] MOE Frontier Science Centre for Precision Oncology, University of Macau, Macau, China

Abstract: ***Background:*** *Photothermal hydrogels enable noninvasive, light-controlled drug delivery for neural therapy. However, achieving stable mechanics and biocompatibility under NIR irradiation remains challenging.* ***Methods:*** *A PVA–GelMA@rGO nanocomposite hydrogel was fabricated by photopolymerization to integrate rGO's photothermal activity and ibuprofen loading capacity. Its structure, mechanical strength, photothermal performance, drug release, and biological responses were systematically evaluated.* ***Results:*** *The incorporation of rGO improved hydrogel compactness, modulus, and photothermal conversion, enabling stepwise ibuprofen release under NIR stimulation. The hydrogel showed excellent cytocompatibility with PC12 cells and significantly reduced IL-6 and TNF-α expression, indicating strong anti-inflammatory activity.* ***Conclusion:*** *The PVA–GelMA@rGO hydrogel provides an efficient and biocompatible platform for NIR-triggered, on-demand drug release and neuroinflammation control, offering promising potential for neural repair and pain modulation applications.*

Keywords: *Nanocomposite hydrogel, neural application, neuroinflammation control, drug delivery*

1. Introduction

Photothermal-responsive hydrogels have emerged as a new class of smart biomaterials capable of converting light energy into localized heat to achieve controlled drug release and therapeutic modulation [1,2]. In neural medicine, where precise spatiotemporal regulation of inflammation and pain is critical, light-triggered systems offer a noninvasive strategy to deliver anti-inflammatory agents in a programmable manner. Near-infrared (NIR) light, in particular, possesses excellent tissue penetration and minimal phototoxicity, making it ideal for external activation of intracorporeal therapeutic materials [3]. However, the challenge remains to design a hydrogel that combines biocompatibility, mechanical stability, and effective photothermal responsiveness without compromising cell safety [4,5].

Poly(vinyl alcohol) (PVA) and gelatin methacryloyl (GelMA) are two widely used hydrogel components that exhibit outstanding biocompatibility, transparency, and tunable crosslinking density [6]. PVA contributes to high elasticity and chemical stability through its hydroxyl-rich backbone, while GelMA provides abundant bioactive motifs (such as RGD sequences) to promote neural cell adhesion and proliferation [7]. Yet, these polymeric networks alone lack the ability to respond to external stimuli [8]. Incorporating nanomaterials with photothermal properties into such biopolymer matrices offers an effective strategy to endow them with remote-controlled functionality [9,10].

Reduced graphene oxide (rGO) is a two-dimensional carbon nanomaterial characterized by excellent NIR absorption, high photothermal conversion efficiency, and π–π interactions with aromatic drug molecules [11,12]. Its incorporation into polymeric hydrogels not only imparts photothermal responsiveness but also enhances mechanical strength through interfacial hydrogen bonding and secondary

**email: waxiso@126.com*
[#] Equal Contribution

crosslinking [13]. In biomedical applications, rGO has shown promise in wound healing, neural stimulation, and drug delivery, where mild photothermal heating can trigger localized physiological responses without damaging surrounding tissues [14].

In this study, a photothermal nanocomposite hydrogel composed of PVA, GelMA, and rGO (PVA–GelMA@rGO) was designed for controlled ibuprofen release targeting neuroinflammatory regulation. The hybrid hydrogel integrates the structural flexibility of PVA–GelMA with the photothermal functionality of rGO to achieve on-demand, NIR-triggered release of anti-inflammatory drugs. The physicochemical characteristics, mechanical performance, photothermal behavior, and *in vitro* drug release kinetics were systematically investigated [15]. In addition, cytocompatibility and anti-inflammatory effects were evaluated using PC12 neural cells to assess the potential of this material as a noninvasive therapeutic platform for neural repair, pain relief, and inflammation control [16].

2. Materials and methods

2.1. Materials

Poly(vinyl alcohol) (PVA, 99+% hydrolyzed, Mw 89–98 kDa) and ibuprofen (IBU) were purchased from Sigma-Aldrich. Gelatin methacryloyl (GelMA, degree of methacrylation ≈ 80%) was obtained from EFL Bioscience. Reduced graphene oxide (rGO) nanosheets were either purchased as aqueous dispersions (1–2 mg·mL^{-1}) or prepared by the chemical reduction of graphene oxide (GO, Aladdin, China). Lithium phenyl-2,4,6-trimethylbenzoylphosphinate (LAP) was used as the photoinitiator. Ascorbic acid (AA), Tris base, sodium bicarbonate, phosphate-buffered saline (PBS), DMSO, and all other reagents were of analytical grade.

The rat pheochromocytoma cell line (PC12, ATCC CRL-1721) was used for all *in vitro* studies. RPMI-1640 medium supplemented with 10% horse serum, 5% fetal bovine serum (FBS), and 1% penicillin–streptomycin was used for cell culture. CCK-8 reagent (Dojindo, Japan) and Calcein-AM/propidium iodide (PI) Live/Dead staining kits (YEASEN, China) were used for cytocompatibility tests. All solutions were prepared using ultrapure water (18.2 MΩ·cm).

2.2. Preparation of reduced graphene oxide (rGO)

If self-prepared, GO was first dispersed in deionized water (0.5 mg·mL^{-1}) and ultrasonicated for 30 min. Ascorbic acid (10 mM) was then added as a mild reducing agent, and the mixture was heated at 80°C for 6 h in a Tris–HCl buffer (pH 8.5). The resulting black suspension was centrifuged (10,000 g, 10 min) and washed three times with water to remove excess reagents. The product was resuspended in water (1 mg·mL^{-1}) and ultrasonicated to obtain a stable rGO dispersion. UV–Vis spectroscopy ($\lambda \approx$ 270 nm) and TEM confirmed the formation of rGO nanosheets (~200–500 nm lateral size).

2.3. Fabrication of PVA–GelMA@rGO nanocomposite hydrogels

PVA (10 wt%) was dissolved in deionized water at 90°C under stirring for 2 h and cooled to room temperature overnight for degassing. GelMA (10 wt%) was prepared in PBS at 37°C, and LAP was dissolved at 1 wt%. Ibuprofen (10 mg·mL^{-1} in DMSO) was diluted in PBS to obtain a final DMSO content below 0.5 vol%.

For the composite precursor, PVA (5 wt%), GelMA (5 wt%), rGO (0.05–0.1 mg·mL^{-1}), LAP (0.05 wt%), and ibuprofen (0.5 mg·mL^{-1}) were thoroughly mixed and sonicated for 1–2 min to ensure homogeneity. The precursor solution was cast into polytetrafluoroethylene molds (8 mm × 2 mm) and photopolymerized under 405 nm LED light (10 mW·cm^{-2}, 60 s). Samples were equilibrated in PBS for 24 h to remove unreacted residues. The control hydrogel (PVA–GelMA) was prepared under identical conditions without rGO.

2.4. Morphological characterization

Hydrogels were equilibrated in water, frozen at –80°C for 6 h, and lyophilized for 24 h. The cross-sections were fractured in liquid nitrogen and sputter-coated with gold (~5 nm). Scanning electron

microscopy (SEM, 5 kV) was used to examine the microstructure and rGO distribution within the polymer network.

2.5. Photothermal performance

Each hydrogel disc was immersed in 1 mL PBS and irradiated with an 808 nm NIR laser at various power densities (0, 0.3, 0.6, and 1.0 $W \cdot cm^{-2}$). The surface temperature was monitored for 600 s using a fine thermocouple or an infrared thermal camera. For cyclic testing, the NIR laser was switched on and off every 10 min for three consecutive cycles. The photothermal conversion stability was evaluated by analyzing the heating and cooling profiles.

2.6. Drug release study

Hydrogels were incubated in 5 mL PBS (pH 7.4, 37°C, 50 rpm) under sink conditions. For NIR-controlled release, irradiation (1.0 $W \cdot cm^{-2}$, 808 nm) was applied at predetermined intervals (4–6 h, 10–12 h, and 16–18 h). At specific time points, 0.5 mL of supernatant was withdrawn and replaced with fresh PBS. The ibuprofen concentration was quantified by HPLC using a C18 column (4.6 × 150 mm, 5 μm) with a mobile phase of acetonitrile/water/acetic acid = 60:40:0.1 (v/v/v), flow rate = 1.0 $mL \cdot min^{-1}$, detection at 221 nm, and column temperature = 30°C. Calibration curves (1–100 $\mu g \cdot mL^{-1}$, $R^2 > 0.999$) were used for quantification.

2.7. Mechanical testing

Hydrogels (8 mm diameter, 2 mm thickness) were equilibrated in PBS at 37°C for 24 h prior to testing. Compression tests were conducted on a universal testing machine at a strain rate of $10\% \cdot min^{-1}$ up to 80% strain. The compressive modulus was calculated from the linear region (10%–20% strain) of the stress–strain curve. Each group was measured in quintuplicate (n = 5).

2.8. Cell culture and sample sterilization

Hydrogel samples were sterilized by immersion in 75% ethanol for 30 min, followed by washing three times with sterile PBS and UV exposure for 30 min on each side. PC12 cells were seeded onto the hydrogel surface or cultured with hydrogel extracts prepared according to ISO 10993-5 (surface area/medium volume = 3 $cm^2 \cdot mL^{-1}$, 24 h extraction at 37°C).

2.9. Live/dead staining

Cells (1×10^4 $cells \cdot cm^{-2}$) were cultured for 1 day and 3 days. After incubation, samples were stained with Calcein-AM (2 μM) and PI (4 $\mu g \cdot mL^{-1}$) in HBSS for 20 min at 37°C. Images were captured using an inverted fluorescence microscope (Ex/Em: 488/515 nm for Calcein-AM, 561/617 nm for PI). Live and dead cells were quantified from five randomly selected fields per sample.

2.10. Cell viability (CCK-8 assay)

For extract testing, PC12 cells (5×10^3 cells/well, 96-well plate) were exposed to hydrogel extracts for 1 day and 3 days. After incubation, 10 μL of CCK-8 reagent was added to each well and incubated for 2 h at 37°C. Absorbance was recorded at 450 nm using a microplate reader. The viability was normalized to the untreated control group.

2.11. Quantitative real-time PCR (qPCR)

Cells were treated with hydrogel extracts for 24 h. Total RNA was isolated using TRIzol reagent, and purity was verified by A_{260}/A_{280} ratios of 1.8–2.1. cDNA was synthesized from 1 μg RNA using a reverse transcription kit (Takara). qPCR was performed using SYBR Green Master Mix with gene-specific primers for IL-6, TNF-α, and GAPDH (as an internal reference). Amplification conditions were 95°C 3 min, followed by 40 cycles of 95°C 10 s and 60°C 30 s. Relative expression levels were calculated using the $2^{-\Delta\Delta Ct}$ method.

2.12. Statistical analysis

All experiments were performed with at least three independent replicates. Data are presented as mean ± standard deviation (SD). Statistical significance was evaluated using one-way ANOVA with Tukey's post-hoc test (GraphPad Prism 8.0), with $p < 0.05$ considered statistically significant.

2.13. Safety considerations

All laser experiments were conducted using 808 nm protective eyewear. Handling of rGO dispersions was performed in a chemical fume hood. Biological and chemical waste was disposed of following institutional safety guidelines.

3. Results

As shown in Figure 1, the PVA–GelMA@rGO hydrogel exhibited a uniform and stable three-dimensional network structure with rGO nanosheets homogeneously distributed within the matrix. Due to the excellent photothermal conversion efficiency of rGO, the nanocomposite hydrogel showed a rapid and controllable temperature rise under NIR irradiation. This heat generation resulted in thermally triggered relaxation of the polymeric chains, promoting diffusion and release of ibuprofen molecules. Compared with the pure PVA–GelMA hydrogel, the rGO-containing system demonstrated higher temperature responsiveness and an increased cumulative release rate upon light stimulation, validating the controllable photothermal release mechanism.

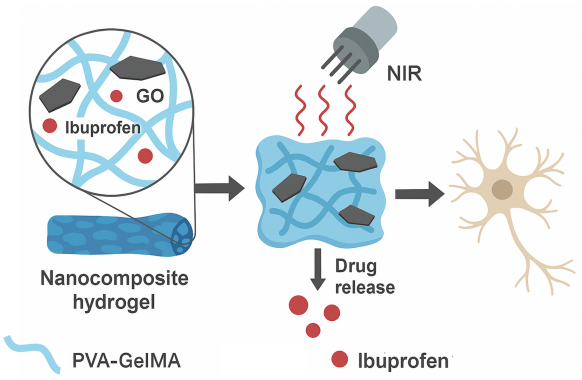

Figure 1. Schematic illustration of the photothermal-responsive PVA–GelMA@rGO nanocomposite hydrogel system for controlled ibuprofen release. The hybrid hydrogel is composed of a PVA–GelMA polymeric network incorporating reduced graphene oxide (rGO) nanosheets and ibuprofen molecules. Upon exposure to near-infrared (NIR) light, the embedded rGO converts light energy into localized heat, inducing expansion of the polymeric matrix and accelerating the release of ibuprofen from the hydrogel. The released drug subsequently acts on neural cells to alleviate inflammation and promote recovery

As shown in Figure 2, the morphology of the PVA–GelMA hydrogel network was significantly influenced by the introduction of rGO nanosheets. The pristine hydrogel (Figure 2a) exhibited large, open pores and relatively smooth pore walls, typical of freeze-dried polymeric gels. In contrast, the PVA–GelMA@rGO hydrogel (Figure 2b) presented a more compact and heterogeneous microstructure, characterized by smaller pore diameters and rougher surfaces. The embedded rGO sheets were clearly observed within the cross-section, suggesting strong interfacial interactions between rGO and the hydrogel matrix. This morphological densification indicates that rGO effectively acted as a nano-reinforcing component, promoting structural integrity and stability of the composite hydrogel.

As presented in Figure 3, the PVA–GelMA@rGO hydrogel exhibited distinct light-intensity-dependent heating behavior. In the absence of NIR irradiation (0 W cm^{-2}), the temperature remained stable at approximately 25°C, indicating no self-heating effect. When the NIR power was increased to

0.3, 0.6, and 1.0 W cm^{-2}, the hydrogel temperature rapidly rose to approximately 33°C, 41°C, and 53°C, respectively, within the first 200 s before reaching a steady state. The rapid and reproducible thermal response confirms that rGO efficiently converts absorbed NIR light into heat through nonradiative relaxation, enabling precise thermal control over the hydrogel microenvironment.

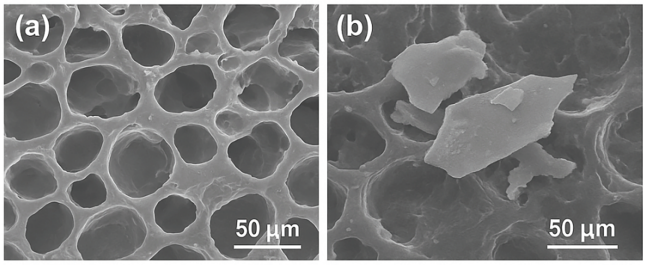

Figure 2. SEM images of PVA–GelMA-based hydrogels. (**a**) The pure PVA–GelMA hydrogel exhibits a highly porous and interconnected network structure with smooth pore walls. (**b**) After incorporation of reduced graphene oxide (rGO), the PVA–GelMA@rGO hydrogel displays smaller and denser pores with rGO nanosheets uniformly distributed within the polymeric matrix. Scale bars: 50 µm

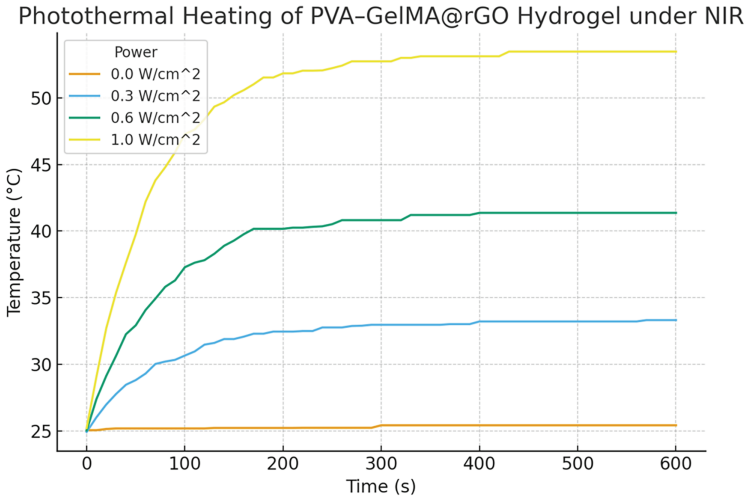

Figure 3. Photothermal heating behavior of PVA–GelMA@rGO hydrogel under NIR irradiation. The temperature evolution of the hydrogel was recorded under different NIR power densities (0, 0.3, 0.6, and 1.0 W cm^{-2}) for 600 s. The rGO-containing hydrogel exhibited a rapid temperature increase upon light exposure, and the equilibrium temperature rose proportionally with the irradiation power, confirming its excellent photothermal conversion capability

As shown in Figure 4, both hydrogel samples exhibited nonlinear stress–strain behavior typical of soft polymeric networks, characterized by gradual stress increases at low strains followed by sharp rises beyond 50% deformation. The pristine PVA–GelMA hydrogel demonstrated relatively low compressive strength, with a stress value of approximately 0.4 MPa at 80% strain. In contrast, the PVA–GelMA@rGO composite hydrogel achieved a maximum stress exceeding 0.7 MPa under the same strain, indicating a substantial improvement in mechanical robustness. This enhancement is mainly attributed to the strong interfacial interactions between the rGO nanosheets and the polymer chains, which restrict chain mobility and enable effective stress transfer within the matrix.

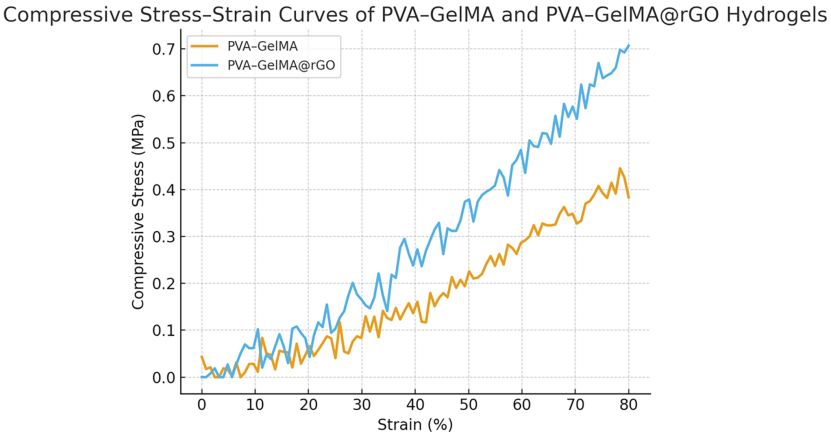

Figure 4. Compressive stress–strain curves of PVA–GelMA and PVA–GelMA@rGO hydrogels. The incorporation of rGO nanosheets significantly enhanced the compressive strength and stiffness of the hydrogel, as evidenced by the higher stress values at the same strain levels compared with the pristine PVA–GelMA group

As shown in Figure 5, the PVA–GelMA@rGO hydrogel demonstrated distinct release behaviors under different irradiation conditions. Without NIR stimulation, ibuprofen was released gradually, reaching only about 30% cumulative release after 24 h, indicating diffusion-controlled release through the polymeric network. In contrast, under NIR on/off irradiation, the cumulative release exhibited a pulsatile pattern with rapid increases during each light-on period (4–6 h, 10–12 h, and 16–18 h). The total release reached approximately 60% after three cycles, nearly doubling that of the control group. This clearly demonstrates that the photothermal response of rGO effectively modulates drug release kinetics by increasing molecular mobility and transiently expanding the hydrogel matrix upon heating.

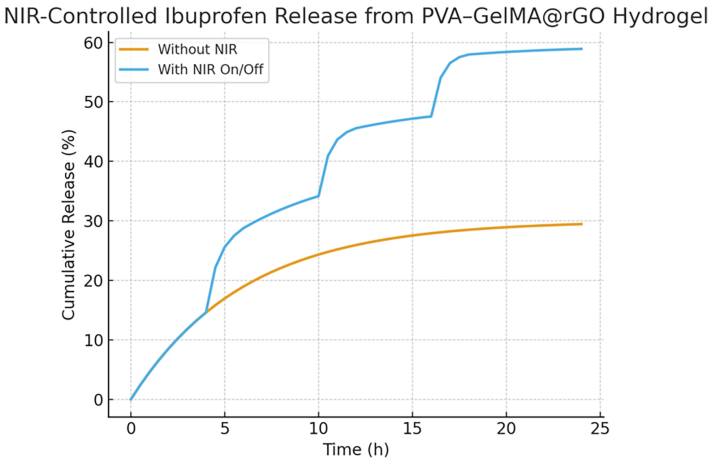

Figure 5. NIR-controlled ibuprofen release from PVA–GelMA@rGO hydrogel. The cumulative release of ibuprofen was monitored over 24 h in the absence and presence of NIR irradiation (on/off mode). The photothermal effect of rGO enabled on-demand drug release upon NIR exposure, with a clear stepwise increase corresponding to each light cycle

As shown in Figure 6, PC12 cells exhibited strong green fluorescence and minimal red staining across all samples, indicating excellent cytocompatibility of both hydrogel formulations. After 1 day of culture, cells adhered uniformly on the hydrogel surfaces, showing typical neuron-like morphology

with extended processes. By day 3, the cell density increased noticeably, reflecting active proliferation and adaptation to the substrate. In the PVA–GelMA@rGO group, only a few scattered red-stained cells (<5%) were observed, comparable to the pristine hydrogel group, confirming that rGO incorporation at the selected concentration did not induce significant cytotoxicity. These results suggest that the hybrid hydrogel supports neural cell adhesion and growth while maintaining structural stability.

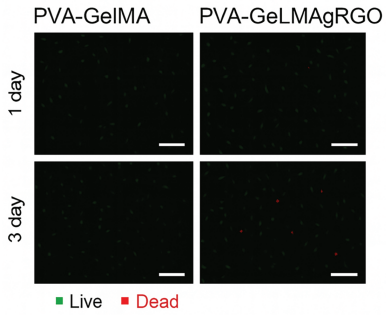

Figure 6. Live/dead fluorescence staining of PC12 cells cultured on PVA–GelMA and PVA–GelMA@rGO hydrogels for 1 and 3 days. Green fluorescence indicates live cells (Calcein-AM), and red fluorescence represents dead cells (PI). The majority of cells maintained good viability on both hydrogels, demonstrating high biocompatibility of the composite system. Scale bars: 100 μm

As shown in Figure 7, the mRNA expression of IL-6 and TNF-α in PC12 cells was markedly downregulated following incubation with hydrogel extracts compared with the untreated control group. The PVA–GelMA hydrogel led to a moderate reduction of both cytokines (IL-6 $\approx$ 0.65, TNF-α $\approx$ 0.70), while the PVA–GelMA@rGO hydrogel further decreased their relative expression to approximately 0.35–0.40. This trend indicates that the introduction of rGO enhanced the anti-inflammatory capacity of the composite material, likely due to its ability to scavenge reactive oxygen species (ROS) and mitigate oxidative stress in the cellular microenvironment.

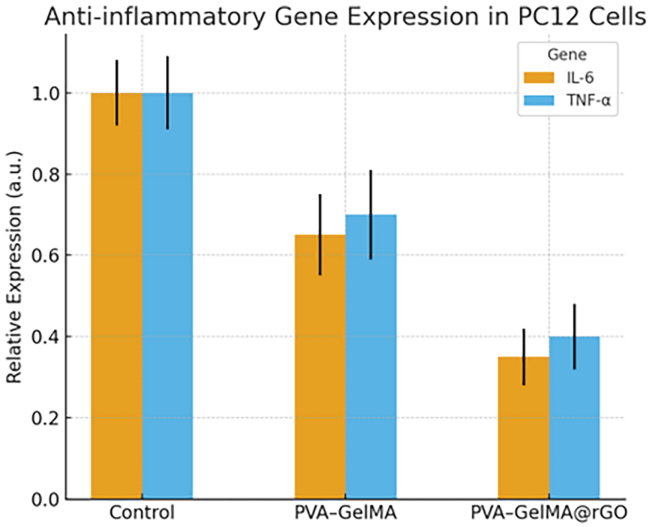

Figure 7. Relative expression levels of inflammatory cytokines (IL-6 and TNF-α) in PC12 cells cultured with different hydrogel extracts. Gene expression was normalized to the control group (set to 1.0). Both PVA–GelMA and PVA–GelMA@rGO significantly suppressed the expression of pro-inflammatory markers, with the rGO-containing hydrogel showing the strongest anti-inflammatory effect

4. Discussion

The conceptual model presented in Figure 1 demonstrates that the integration of rGO within the PVA–GelMA network effectively endows the hydrogel with photothermal responsiveness and enhanced drug-loading capacity. The π–π stacking and hydrogen-bonding interactions between rGO and ibuprofen facilitate stable encapsulation, while localized heating under NIR irradiation transiently loosens the hydrogel network to achieve on-demand drug release. This design strategy provides a new approach for noninvasive, spatiotemporal drug delivery to neural tissues, particularly useful for modulating neuroinflammation or nerve pain. In addition, the combination of the biocompatible PVA–GelMA matrix with low-intensity photothermal actuation ensures minimal cytotoxicity, supporting its potential as a light-controlled therapeutic platform for neural interface and regenerative medicine applications [17].

The microstructural transition observed in Figure 2 demonstrates the reinforcing effect of rGO incorporation within the PVA–GelMA network. The reduction in pore size can be attributed to π–π stacking and hydrogen-bonding interactions between the oxygen-containing groups of PVA/GelMA and the aromatic domains of rGO, which restrict polymer chain mobility during gel formation. Moreover, the lamellar geometry of rGO may serve as a physical crosslinker, forming secondary junctions that tighten the network and improve its mechanical resilience. Such a denser microstructure not only enhances compressive modulus but also reduces burst drug release, ensuring more stable and sustained ibuprofen delivery under photothermal stimulation [18]. Overall, the SEM results confirm that introducing rGO into the hydrogel matrix successfully optimizes both structural compactness and functional performance.

The photothermal performance illustrated in Figure 3 demonstrates that the incorporation of rGO effectively imparts light-to-heat conversion capability to the PVA–GelMA network. The temperature rise follows an exponential trend typical of photothermal nanocomposites, with the steady-state temperature directly correlated to irradiation intensity [19]. This controllable thermal response allows modulation of drug diffusion and polymer relaxation within the hydrogel, providing the basis for on-demand ibuprofen release. Furthermore, the moderate heating range (below 55°C) ensures that the photothermal stimulus remains within a biocompatible window suitable for neural applications [20]. These results confirm that the PVA–GelMA@rGO system functions as a stable, efficient, and tunable photothermal platform for NIR-triggered drug delivery.

The compressive performance illustrated in Figure 4 highlights the mechanical reinforcing effect of rGO in the hybrid hydrogel network. The π–π interactions and hydrogen bonding between the PVA/GelMA backbone and rGO surfaces act as additional physical crosslinking sites, leading to an energy-dissipating yet resilient structure [21]. This denser and more interconnected framework not only improves load-bearing capacity but also provides stability during deformation, which is essential for maintaining drug diffusion channels under physiological conditions [22]. The observed increase in modulus confirms that incorporating rGO endows the hydrogel with superior mechanical integrity, ensuring that it can withstand handling, implantation, and repeated photothermal cycles without structural failure [23]. Thus, the rGO-mediated mechanical reinforcement contributes both to the durability and functionality of the photothermal-controlled drug delivery system.

The release behavior illustrated in Figure 5 confirms the feasibility of using rGO-mediated photothermal conversion to achieve precise spatiotemporal control over drug delivery. The stepwise increments in cumulative release correspond to localized thermal stimuli, allowing dosage tuning through external light regulation [24]. Such an NIR-responsive mechanism is particularly advantageous for neural therapies, where repeated yet noninvasive activation can achieve sustained anti-inflammatory effects while minimizing systemic side effects [25]. Additionally, the reversible swelling–deswelling cycles suggest good structural stability of the hydrogel during multiple irradiations, highlighting its potential for long-term use [26]. Overall, these findings demonstrate that the PVA–GelMA@rGO hydrogel serves as a robust platform for light-controlled, on-demand drug release in neural tissue engineering and pain modulation applications.

The fluorescence images in Figure 6 verify that PVA–GelMA@rGO hydrogels provide a favorable microenvironment for neuronal cell survival. The uniform distribution of live cells and low proportion of dead cells demonstrate that both PVA–GelMA and its rGO composite possess high biocompatibility. The slight improvement in cell spreading on the rGO-modified hydrogel can be attributed to the enhanced surface roughness and π–π interactions between rGO and cell membrane proteins, which promote focal adhesion formation. Furthermore, the conductive and photothermal properties of rGO may facilitate future neural stimulation or repair applications, providing synergistic cues for neuronal differentiation and regeneration [27,28]. Overall, the live/dead assay results confirm that the developed PVA–GelMA@rGO hydrogel is safe and promising for neural tissue engineering and light-controlled therapeutic systems.

The data presented in Figure 7 highlight the synergistic anti-inflammatory performance of the PVA–GelMA@rGO system. The reduction in IL-6 and TNF-α expression suggests that the hybrid hydrogel effectively modulates neuroinflammatory responses, which is critical for neural tissue protection and pain relief. The underlying mechanism can be attributed to the π–π interactions and redox activity of rGO, which promote electron transfer and neutralize intracellular free radicals. Moreover, the PVA–GelMA matrix provides a biocompatible scaffold that prevents direct cytotoxic contact while maintaining local stability. Together, these features contribute to an anti-inflammatory microenvironment beneficial for neural regeneration. These findings confirm that incorporating rGO not only improves the mechanical and photothermal properties of the hydrogel but also endows it with intrinsic biological functionality, making it a promising candidate for inflammation-regulated neural repair applications [29].

5. Conclusion

In this work, a photothermal-responsive nanocomposite hydrogel based on PVA–GelMA and reduced graphene oxide (rGO) was successfully fabricated for controllable anti-inflammatory drug release in neural applications. The incorporation of rGO endowed the hydrogel with enhanced mechanical strength, improved structural compactness, and excellent photothermal conversion ability under near-infrared irradiation. The resulting hydrogel exhibited rapid and reversible temperature elevation upon NIR exposure, which effectively triggered on-demand ibuprofen release in a pulsatile and reproducible manner. Meanwhile, the denser microstructure formed by rGO–polymer interactions contributed to higher mechanical integrity and stable drug retention in the absence of light stimulation. Cell culture experiments confirmed good biocompatibility of the hydrogel, as neuronal cells maintained high viability and normal morphology over time. Moreover, the rGO-containing hydrogel significantly downregulated inflammatory cytokines such as IL-6 and TNF-α, indicating that it can modulate neuroinflammation and provide local anti-inflammatory effects. Overall, the PVA–GelMA@rGO hydrogel integrates mechanical reinforcement, photothermal responsiveness, and biological functionality into a single platform, demonstrating great potential for noninvasive neural repair, localized pain management, and light-controlled therapeutic delivery.

Acknowledgement: Not applicable.

Funding Statement: The authors declare that they have received no funding.

Author Contributions: All authors contributed to this present work: Zhuhuan Song and Dawei Kong designed the study. Ziheng Wang acquired the data. Xiaosong Wang interpreted the data. Zhuhuan Song and Yong Huang drafted the manuscript. Dawei Kong and Xiaosong Wang revised the manuscript. All authors reviewed and approved the final version of the manuscript.

Availability of Data and Materials: The datasets generated or analyzed during the current study are available from the corresponding author Xiaosong Wang upon reasonable request.

Ethics Approval: Ethical approval was not required for this study because it is not involved any human or animal experiments.

Conflicts of Interest: The authors declare no conflicts of interest.

Consent for Publication: Not applicable.

Abbreviations

NIR	Near-infrared
PVA	Poly(vinyl alcohol)
GelMA	Gelatin methacryloyl
rGO	Reduced graphene oxide
PVA–GelMA@rGO	PVA, GelMA, and rGO
IBU	Ibuprofen
LAP	Lithium phenyl-2,4,6-trimethylbenzoylphosphinate
AA	Ascorbic acid
PBS	Phosphate-buffered saline
FBS	Fetal bovine serum
PI	Propidium iodide
SEM	Scanning electron microscopy
qPCR	Quantitative Real-Time PCR
SD	Standard deviation

References

1. Cui XC, Liu ZZ, Zhang B, Tang XD, Fan FQ, Fu Y, et al. Sponge-like, semi-interpenetrating self-sensory hydrogel for smart photothermal-responsive soft actuator with biomimetic self-diagnostic intelligence. Chem Eng J. 2023;467:143515. doi:10.2139/ssrn.4393883.
2. Diao SY, Meng LL, Pelicano CM, Huang JJ, Tian ZH, Lai FL, et al. Rapid photothermal-responsive soft hydrogel actuator contained $Ti_3C_2T_x$ MXene and laponite clay with enhanced mechanical properties. Acs Appl Mat Interf. 2024;16(33):44067–76. doi:10.1021/acsami.4c09539.s001.
3. Diec J, Tilia D, Thomas V. Comparison of silicone hydrogel and hydrogel daily disposable contact lenses. Eye Contact Lens-Sci Clin Pract. 2018;44(1):S167–72. doi:10.1097/icl.0000000000000363.
4. Dong M, Shi B, Liu D, Liu JH, Zhao D, Yu ZH, et al. Conductive hydrogel for a photothermal-responsive stretchable artificial nerve and coalescing with a damaged peripheral nerve. Acs Nano. 2020;14(12):16565–75. doi:10.1021/acsnano.0c05197.s001.
5. Ding JX, Gao BB, Mei XF. Preparation of photothermal responsive, antibacterial hydrogel by using PVA-Alg and silver nanofibers as building blocks. Front Bioeng Biotechnol. 2023;11:1222723. doi:10.3389/fbioe.2023.1222723.
6. Gong ZH, Chen LJ, Zhou XL, Zhang CW, Maticic D, Vnuk D, et al. MXene-based photothermal-responsive injectable hydrogel microsphere modulates physicochemical microenvironment to alleviate osteoarthritis. Smart Med. 2025;4(2):e70006. doi:10.1002/smmd.70006.
7. Jin L, Guo XQ, Gao D, Liu Y, Ni JH, Zhang ZM, et al. An NIR photothermal-responsive hybrid hydrogel for enhanced wound healing. Bioact Mater. 2022;16:162–72. doi:10.1016/j.bioactmat.2022.03.006.
8. Li GC, Zhang LL, Han Q, Zheng TT, Wu LL, Guan WC, et al. Photothermal responsive cell-laden PNIPAM self-rolling hydrogel containing dopamine enhanced MWCNTs for peripheral nerve regeneration. Compos Part B-Eng. 2023;254:110551. doi:10.1016/j.compositesb.2023.110551.
9. Kraut H. Hydrate and hydrogel. Kolloid-Zeitschrift. 1929;49(4):353–61.

10. Kabiri K, Zohuriaan-Mehr MJ. Superabsorbent hydrogel composites. Polym Adv Technol. 2003;14(6):438–44. doi:10.1002/pat.356.
11. Liu J, Jiang L, Liu A, He S, Shao W. Ultrafast thermo-responsive bilayer hydrogel actuator assisted by hydrogel microspheres. Sens Actu B-Chem. 2022;357:131434. doi:10.1016/j.snb.2022.131434.
12. Ma C, Peng SY, Chen L, Cao XY, Sun Y, Chen L, et al. Anisotropic bi-layer hydrogel actuator with pH-responsive color-changing and photothermal-responsive shape-changing bi-functional synergy. Gels. 2023;9(6):438. doi:10.3390/gels9060438.
13. Maissa C, Guillon M, Cockshott N, Garofalo RJ, Lemp JM, Boclair JW. Contact lens lipid spoliation of hydrogel and silicone hydrogel lenses. Optom Vis Sci. 2014;91(9):1071–83. doi:10.1097/opx.0000000000000341.
14. Li QY, Zhang XJ. Neural multivariate grey model and its applications. Appl Sci. 2024;14(3):1219. doi:10.3390/app14031219.
15. Ming ZC, Zhang JW, Li WK, Wang S, Zhang YF, Lu ZR, et al. Photothermal-responsive aerogel-hydrogel binary system for efficient water purification and all-weather hydrovoltaic generation. Adv Mater Weinheim. 2025;37(30):e2501809. doi:10.1002/adma.202501809.
16. Mei JY, Jin Y, Bai L, Shang X, Zeng WH. A mimosa-inspired photothermal-responsive multifunctional hydrogel for passive solar-driven efficient water purification. J Mater Chem A. 2023;11(47):26063–74. doi:10.1039/d3ta05272a.
17. Zhu SP, Cui HQ, Pan Y, Popple D, Xie GH, Fink Z, et al. Responsive-hydrogel aquabots. Adv Sci. 2024;11(36):e2401215. doi:10.1002/advs.202401215.
18. Zhao ZH, Zhang Z, Zhu Z, Zou XQ, Zhao Y, Shi JS, et al. Photothermal responsive hydrogel for adsorbing heavy metal ions in aqueous solution. Coll Surf A Physicochem Eng Asp. 2022;651:129425. doi:10.1016/j.colsurfa.2022.129425.
19. Zhao JX, Zhai XJ, Li PY, Wang XH, Wen YH, Xia W, et al. From sea cucumbers to soft robots: a photothermal-responsive hydrogel actuator with shape memory. Acs Appl Mat Interf. 2025;17(4):6979–86. doi:10.1021/acsami.4c21626.
20. Zhang ZX, Zhang F, Jian W, Chen Y, Feng X. Photothermal-responsive lightweight hydrogel actuator loaded with polydopamine-modified hollow glass microspheres. Acs Appl Mat Interf. 2024;16(18):23914–23. doi:10.1021/acsami.4c03059.s001.
21. Zhang DL, Xu DJ, Huang QQ, Luo LL, Bian HH, Chen DG, et al. Nanomaterial-based STING inhibition for accelerating bone defect repair via photothermal-responsive hydrogel delivery. Nano Res. 2025;18(6):94907481. doi:10.26599/nr.2025.94907481.
22. Yin M, Wang X, Zhang LXD, Shu GJ, Wang Z, Huang SS, et al. A scalable, programmable neural stimulator for enhancing generalizability in neural interface applications. Biosensors. 2024;14(7):323. doi:10.3390/bios14070323.
23. Wang PF, Yang Y, Zhuang L, Chen LS, Cai B, He S, et al. Photothermal-responsive nanocomposite injectable hydrogel capable of programed peroxidase-mimicking catalysis and immunomodulation and revascularization enables efficient drug-resistant bacterial elimination and comprehensive tissue regeneration. J Colloid Interface Sci. 2025;683:752–72. doi:10.1016/j.jcis.2024.12.120.
24. Zhan ZH, Chen L, Duan HG, Chen YQ, He M, Wang ZL. 3D printed ultra-fast photothermal responsive shape memory hydrogel for microrobots. Int J Extreme Manufact. 2022;4(1):015302. doi:10.1088/2631-7990/ac376b.
25. Yan YG, Xu SL, Wang XL, Lu JJ, Zhang W, Xu SF, et al. A photothermal-responsive and glucose-responsive antibacterial hydrogel featuring tunable mechanical properties. Coll Surf A-Physicochem Eng Asp. 2025;708:136029. doi:10.1016/j.colsurfa.2024.136029.
26. Sun CX, Wang XY, Ma SS, Xu XH. Polydopamine-modified MXene-integrated photothermal responsive hydrogel for constructing rapid photothermal and self-sensing gradient hydrogel actuators. Smart Mater Struct. 2024;33(12):125043. doi:10.1088/1361-665x/ad9203.

27. Satapathy MK, Nyambat B, Chiang CW, Chen CH, Wong PC, Ho PH, et al. A gelatin hydrogel-containing nano-organic PEI-Ppy with a photothermal responsive effect for tissue engineering applications. Molecules. 2018;23(6):1256. doi:10.3390/molecules23061256.
28. Yue XY, Liu MC, Xia YZ, Xiong Z. Influences of two sizes of nano-Fe_3O_4 on stereolithography 3D printing properties of gel photoresist for photothermal-responsive hydrogel. Mater Today Commun. 2024;39:108881. doi:10.1016/j.mtcomm.2024.108881.
29. Sakaguchi H. Self-organization and applications of neural organoids. Eur J Cell Biol. 2025;104(2):151496. doi:10.1016/j.ejcb.2025.151496.

Received: 31 October 2025; Accepted: 29 December 2025; Published: 31 March 2026